# Robust Multi-Frequency GPR Microwave Imaging through Multi-Scaling Particle Swarm Optimization

M. Salucci, L. Poli, N. Anselmi, and A. Massa

## Abstract

In this work, an innovative *GPR* microwave imaging technique is proposed for solving the subsurface inverse scattering problem in a multi-frequency (*MF*) framework. The proposed technique exploits a stochastic optimizer based on particle swarm optimization (*PSO*) in order to effectively deal with the minimization of the *MF* cost function without being trapped into false solutions. Moreover, the iterative multi-scaling approach (*IMSA*) is exploited in order to achieve higher resolutions within the identified regions of interest. Some numerical results are shown, carefully selected from an extensive validation of the method, in order to assess its performance when dealing with the retrieval of buried objects under several noise levels. More precisely, a variation of the number of measurement points placed above the interface to collect the scattered radargram is considered, in order to investigate the robustness of the developed method, as well as to compare it to a deterministic implementation within the same solution  framework.

# 1 Definitions

## 1.1 Glossary

- $SF$: Single-Frequency;

- $FH$: Frequency-Hopping;

- $MF$: Multi-Frequency;

- $P$: Swarm dimension;

- $U$: Total number of unknowns;

- $S$: Maximum number of $IMSA$ zooming steps;

- $s^{best}$: Last performed $IMSA$ zooming step ($s^{best} \leq S$);

- $\eta_{th}$: $IMSA$ zooming threshold;

- $D_{inv}$: Investigation domain;

- $D_{obs}$: Observation domain;

- $L$: Side of the investigation domain;

- $N$: Number of discretization cells in $D_{ind}$;

- $V$: Number of views;

- $M$: Number of measurement points;

- $F$: Number of frequencies considered for the inversion;

- $\mathbf{r}^{(v)} = \left(x^{(v)}, y^{(v)}\right)$: Coordinates of the $v$-th source ($v = 1, \ldots, V$).

- $\mathbf{r}_m^{(v)} = \left(x_m^{(v)}, y_m^{(v)}\right)$: Coordinates of the $m$-th measurement point for the $v$-th view $v$, ($m = 1, \ldots, M$);

- $\varepsilon_{ra} = \frac{\varepsilon_a}{\varepsilon_0}$: Relative electric permittivity for the upper half-space ($y > 0$);

- $\sigma_a$: Conductivity for the upper half-space ($y > 0$);

- $\varepsilon_{rb} = \frac{\varepsilon_b}{\varepsilon_0}$: Background relative electric permittivity;

- $\sigma_b$: Background conductivity;

- $E_{inc}^{(v)}\left(\mathbf{r}_n; f\right)$: Measured internal incident field inside the $n$-th cell, for the $v$-th view at frequency $f$;

- $\widetilde{E}_{inc}^{(v)}\left(\mathbf{r}_n; f\right)$: Computed internal incident field inside the $n$-th cell, for the $v$-th view at frequency $f$;

- $E_{scatt}^{(v)}\left(\mathbf{r}_m^{(v)}; f\right)$: Measured external scattered by the $m$-th measurement point, for the $v$-th view at frequency $f$;

- $\widetilde{E}_{scatt}^{(v)}\left(\mathbf{r}_m^{(v)}; f\right)$: Measured external scattered by the $m$-th measurement point, for the $v$-th view at frequency $f$.

## 1.2   Contrast function

The contrast function at frequency $f$ is defined as

$$\tau\left(\mathbf{r};f\right) = \frac{\varepsilon_{eq}\left(\mathbf{r}\right) - \varepsilon_{eqb}}{\varepsilon_0} = \left[\varepsilon_r\left(\mathbf{r}\right) - \varepsilon_{rb}\right] + j\left[\frac{\sigma_b - \sigma\left(\mathbf{r}\right)}{2\pi f \varepsilon_0}\right]$$

where

- $\mathbf{r} = (x, y)$: position vector;

- $\Re\left\{\tau\left(\mathbf{r};f\right)\right\} = \left[\varepsilon_r\left(\mathbf{r}\right) - \varepsilon_{rb}\right]$ ;

- $\Im\left\{\tau\left(\mathbf{r};f\right)\right\} = \left[\frac{\sigma_b - \sigma(\mathbf{r})}{2\pi f \varepsilon_0}\right]$;

- $\varepsilon_{eq}\left(\mathbf{r}\right) = \varepsilon_0 \varepsilon_r\left(\mathbf{r}\right) - j\frac{\sigma(\mathbf{r})}{2\pi f}$ ;

- $\varepsilon_{eqb} = \varepsilon_0 \varepsilon_{rb} - j\frac{\sigma_b}{2\pi f}$;

- $\varepsilon_r\left(\mathbf{r}\right)$: relative electric permittivity at position $\mathbf{r}$;

- $\sigma\left(\mathbf{r}\right)$: conductivity at position $\mathbf{r}$;

**NOTE:** we assume that $\varepsilon_r\left(\mathbf{r}\right)$ and $\sigma\left(\mathbf{r}\right)$ are **not frequency dependent** (non-dispersive mediums).

### 1.2.1   Contrast function and reference frequency $f_{ref}$ ($MF$ approaches)

The contrast function at a generic frequency $f$ can be expressed by means of the contrast function computed for a selected reference frequency

$$f = f_{ref} \tag{1}$$

as follows

$$\tau\left(\mathbf{r};f\right) = \Re\left\{\tau\left(\mathbf{r};f_{ref}\right)\right\} + j\frac{f_{ref}}{f}\Im\left\{\tau\left(\mathbf{r};f_{ref}\right)\right\}. \tag{2}$$

This allows to reduce the number of unknowns when dealing with multi-frequency techniques, since we can just consider the contrast function at the reference frequency.

## 1.3 Cost function & unknowns

### 1.3.1 Multi-Frequency ($MF$) approaches

These approaches jointly consider data at $F$ frequencies. The functional minimized by the inversion algorithm is defined as

$$\Phi\left(\mathbf{x}\right) = \Phi_{state}\left(\mathbf{x}\right) + \Phi_{data}\left(\mathbf{x}\right) \tag{3}$$

where $\Phi_{state}\left(\mathbf{x}\right)$ and $\Phi_{data}\left(\mathbf{x}\right)$ are respectively the data and state terms of the cost function, defined as

$$\Phi_{state}\left(\mathbf{x}\right) = \frac{\sum_{j=1}^{F}\sum_{v=1}^{V}\sum_{n=1}^{N}\left|E_{inc}^{(v)}\left(\mathbf{r}_n;f_j\right) - \widetilde{E}_{inc}^{(v)}\left(\mathbf{r}_n;f_j\right)\right|^2}{\sum_{j=1}^{F}\sum_{v=1}^{V}\sum_{n=1}^{N}\left|E_{inc}^{(v)}\left(\mathbf{r}_n;f_j\right)\right|^2} \tag{4}$$

$$\Phi_{data} = \frac{\sum_{j=1}^{F}\sum_{v=1}^{V}\sum_{m=1}^{M}\left|E_{scatt}^{(v)}\left(\mathbf{r}_m^{(v)};f_j\right) - \widetilde{E}_{scatt}^{(v)}\left(\mathbf{r}_m^{(v)};f_j\right)\right|^2}{\sum_{j=1}^{F}\sum_{v=1}^{V}\sum_{m=1}^{M}\left|E_{scatt}^{(v)}\left(\mathbf{r}_m^{(v)};f_j\right)\right|^2} \tag{5}$$

The unknowns of the inversion problem are

$$\mathbf{x} = \left\{\tau\left(\mathbf{r};f_{ref}\right); E_{tot}^{(v)}\left(\mathbf{r}_n;f_j\right)\right\} \qquad n = 1,...,N; v = 1,...,V; j = 1,...,F. \tag{6}$$

The total number of unknowns for $MF$-based approaches is then given by

$$U_{MF} = 2N\left(1 + VF\right). \tag{7}$$

## 1.4 Reconstruction errors

The following integral error is defined

$$\Xi_{reg} = \frac{1}{N_{reg}}\sum_{n=1}^{N_{reg}}\frac{\left|\tau_n^{act} - \tau_n^{rec}\right|}{\left|\tau_n^{act} + 1\right|} \tag{8}$$

where $reg$ indicates if the error computation covers

- the overall investigation domain ($reg \Rightarrow tot$),

- the actual scatterer support ($reg \Rightarrow int$),

- or the background region ($reg \Rightarrow ext$).

3

# 2 Increasing the number of measurement points ($M$)

## 2.1 Circular empty object ($\varepsilon_{r,obj} = 4.5$, $\sigma_{obj} = 10^{-3}$ [S/m])

### 2.1.1 Parameters

**Background**

Inhomogeneous and nonmagnetic background composed by two half spaces

- Upper half space ($y > 0$ - air): $\varepsilon_{ra} = 1.0$, $\sigma_a = 0.0$;

- Lower half space ($y < 0$ - soil): $\varepsilon_{rb} = 4.0$, $\sigma_b = 10^{-3}$[S/m];

**Investigation domain** ($D_{inv}$)

- Side: $L_{D_{inv}} = 0.8$ [m];

- Barycenter: $\left( x_{bar}^{D_{inv}}, y_{bar}^{D_{inv}} \right) = (0.00, -0.4)$ [m];

**Time-Domain forward solver** ($FDTD$ - $GPRMax2D$)

- Side of the simulated domain: $L = 6$ [m];

- Number of cells: $N^{FDTD} = 750 \times 750 = 5.625 \times 10^5$;

- Side of the $FDTD$ cells $l^{FDTD} = 0.008$ [m];

- Simulation time window: $T^{FDTD} = 20 \times 10^{-9}$ [sec];

- Time step: $\Delta t^{FDTD} = 1.89 \times 10^{-11}$ [sec];

- Number of time samples: $N_t^{FDTD} = 1060$;

- Boundary conditions: perfectly matched layer ($PML$);

- Source type: Gaussian mono-cycle (first Gaussian pulse derivative, called "Ricker" in $GPRMax2D$)

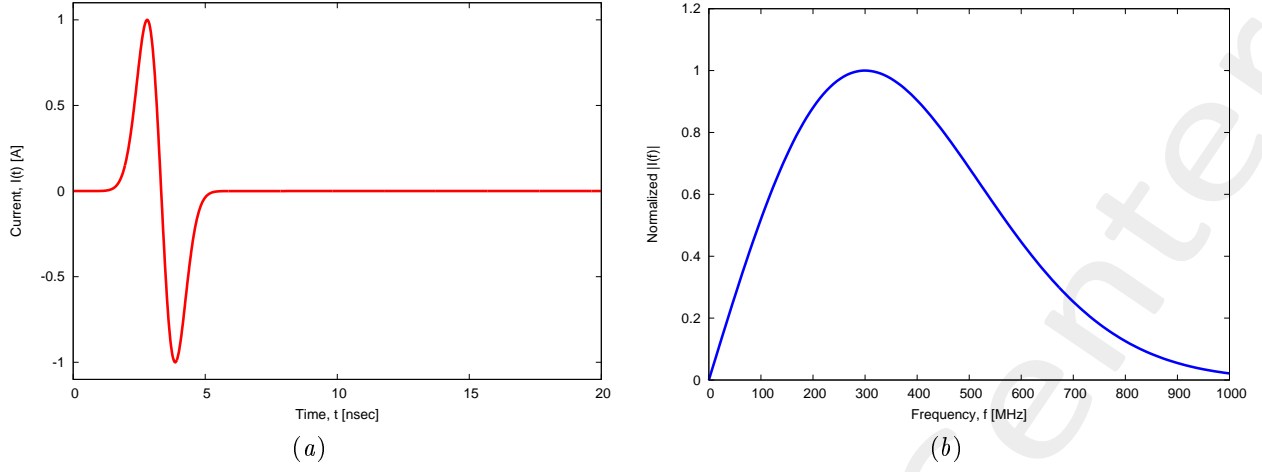  - Central frequency: $f_0 = 300$ [MHz];

  - Source amplitude: $A = 1.0$ [A];

Figure 1: $GPRMax2D$ excitation signal. $(a)$ Time pulse, $(b)$ normalized frequency spectrum.

**Frequency parameters**

- Frequency range: $f \in [f_{min}, f_{max}] = [200.0, 600.0]$ [MHz] $(-3$ [dB] bandwidth of the Gaussian Monocycle excitation centered at $f_0 = 300$ [MHz]);

- Frequency step: $\Delta f = 100$ [MHz] $(F = 5$ frequency steps in $[f_{min}, f_{max}]$);

| $f$ [MHz] | $\lambda_a$ [m] | $\lambda_b$ [m] | $f^*$ [MHz] |
|-----------|-----------------|-----------------|-------------|
| 200.0     | 1.50            | 0.75            | 200.5       |
| 300.0     | 1.00            | 0.50            | 297.6       |
| 400.0     | 0.75            | 0.37            | 401.1       |
| 500.0     | 0.60            | 0.30            | 498.1       |
| 600.0     | 0.50            | 0.25            | 601.6       |

Table 1: Considered frequencies and corresponding wavelength in the upper medium ($\lambda_a$, free space) and in the lower medium ($\lambda_b$, soil). $f^*$ is the nearest frequency sample available from transformed time-domain data, and represents the real frequency considered by the inversion algorithm.

**Scatterer**

- Type: Circular;

- Barycenter: $(x_{obj}, y_{obj}) = (0.0, -0.4)$ [m];

- Radius: $r_{obj}^{int} = 0.08$ [m], $r_{obj}^{ext} = 0.12$ [m];

- Electromagnetic properties: $\varepsilon_{r,obj} = 4.5$, $\sigma_{obj} = 10^{-3}$ [S/m] $(\sigma_{obj} = \sigma_b)$;
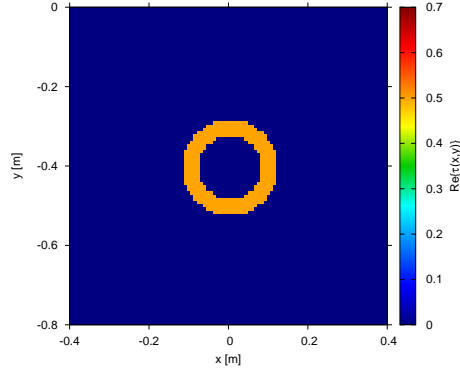
- Contrast function: $\tau = 0.5 + j0.0$

5

Figure 2: Actual object.

**Measurement setup**

- Considered frequency: $f_{min} = 200$ [MHz], $\lambda_b = 0.75$ [m]. [1]

- $\#DoFs = 2ka = \frac{2\pi}{\lambda_b}L\sqrt{2} = \frac{2\pi}{0.75}0.8\sqrt{2} \simeq 9.5$;

- Number of views (sources): $V = 10$;

  - $\min\{x_v\} = -0.5$ [m], $\max\{x_v\} = 0.5$ [m];

  - height: $y_v = 0.1$ [m], $\forall v = 1, \ldots, V$;

- Number of measurement points: $M = \{9; 18; 36; 72\}$;

  - $\min\{x_m\} = -0.5$ [m], $\max\{x_m\} = 0.5$ [m];
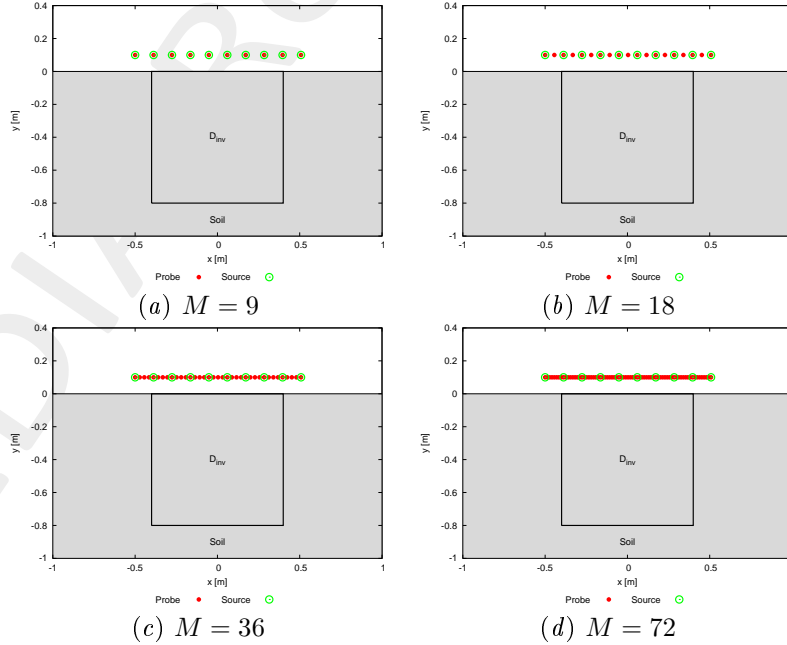
  - height: $y_m = 0.1$ [m], $\forall m = 1, \ldots, M$;



(a) $M = 9$

(b) $M = 18$

(c) $M = 36$

(d) $M = 72$

Figure 3: Location of the measurement points and of the sources ($V = 10$). Only one source is active for each view.

---

[1]**NOTE:** This choice is done in order to keep the number of unknowns lower than 5000.

**Inverse solver parameters**

- **Shared parameters**

  - Number of unknowns: $U = 2N\left(1 + VF\right) = 4998$;

  - Weight of the state term of the functional: $1.0$;

  - Weight of the data term of the functional: $1.0$;

  - Weight of the penalty term of the functional: $0.0$;

  - Convergence threshold: $10^{-10}$;

  - Variable ranges:

    * $\sigma \in \left[8.0 \times 10^{-4}, 1.2 \times 10^{-3}\right]$ [S/m];

    * $\Re\left\{E_{tot}^{int}\right\} \in [-8, 8]$, $\Im\left\{E_{tot}^{int}\right\} \in [-8, 8]$;

  - Degrees of freedom:

    * Considered frequency: $f_{min} = 200$ [MHz], $\lambda_b = 0.75$ [m];
    * $\frac{(2ka)^2}{2} = \frac{\left(2 \times \frac{2\pi}{\lambda_b} \times \frac{L\sqrt{2}}{2}\right)^2}{2} = 4\pi^2\left(\frac{L}{\lambda_b}\right)^2 = 4\pi^2\left(\frac{0.8}{0.75}\right)^2 \simeq 44.87$;

  - Number of cells: $N = 49 = 7 \times 7$;

  - Maximum number of $IMSA$ steps: $S = 4$;

  - Side ratio threshold: $\eta_{th} = 0.2$;

- $MF - IMSA - PSO$ **parameters**

  - Maximum number of iterations: $I = 20000$;

  - Swarm dimension: $P = \frac{5}{100} \times U = 250$;

  - $C_1 = C_2 = 2.0$;

  - Inertial weight: $w = 0.4$;

  - Velocity clamping: enabled;

- $MF - IMSA - CG$ **parameters**

  - Maximum number of iterations: $I = 200$;

**Signal to noise ratio (on $E_{tot}\left(t\right)$)**

- $SNR = \{50, 40, 30, 20\}$ [dB] + Noiseless data.

($a$) Actual

MF-IMSA-PSO — MF-IMSA-CG

($b$) $s^{best} = 4$     ($c$) $s^{best} = 4$

($d$) $s^{best} = 4$     ($e$) $s^{best} = 4$

($f$) $s^{best} = 4$     ($g$) $s^{best} = 4$

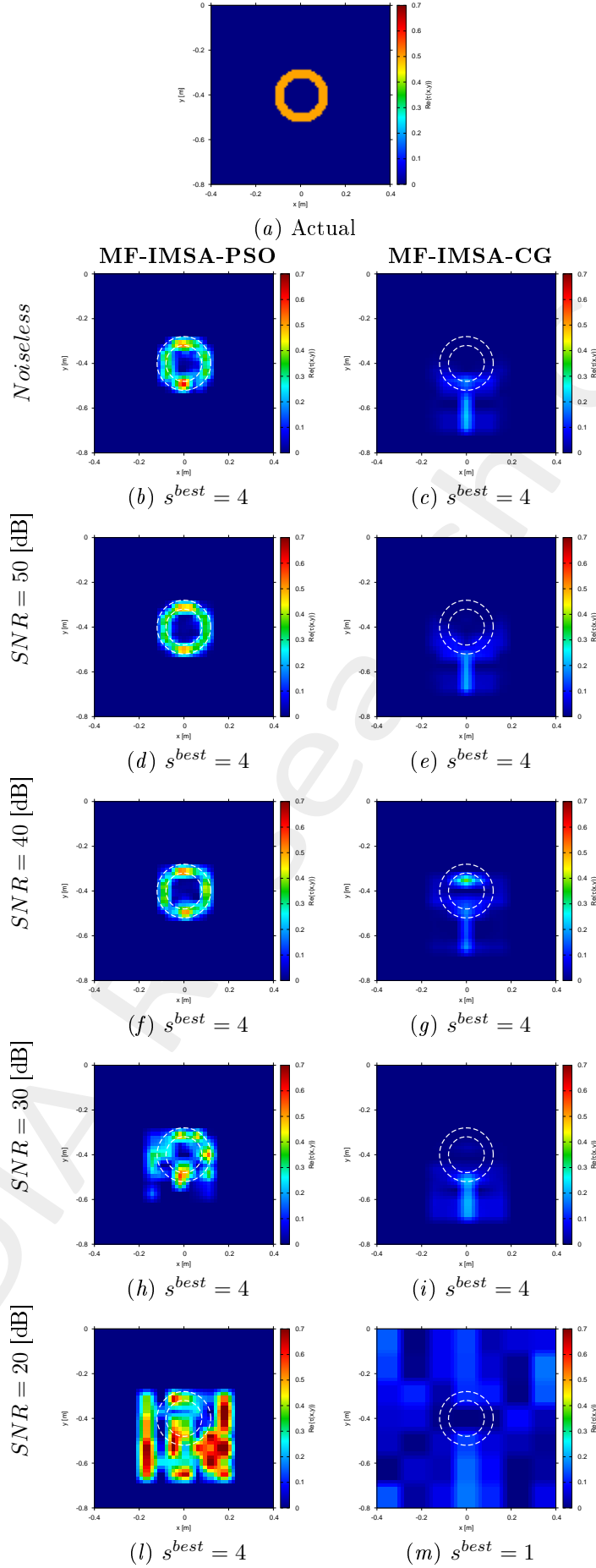($h$) $s^{best} = 4$     ($i$) $s^{best} = 4$

($l$) $s^{best} = 4$     ($m$) $s^{best} = 1$

Figure 4: $MF - IMSA - PSO$ vs. $MF - IMSA - CG$: Retrieved dielectric profiles at the $IMSA$ convergence step ($s^{best}$).

8

$(a)$ Actual

**MF-IMSA-PSO**        **MF-IMSA-CG**

$(b)$ $s^{best} = 4$        $(c)$ $s^{best} = 4$

$(d)$ $s^{best} = 4$        $(e)$ $s^{best} = 4$

$(f)$ $s^{best} = 4$        $(g)$ $s^{best} = 4$

$(h)$ $s^{best} = 4$        $(i)$ $s^{best} = 4$
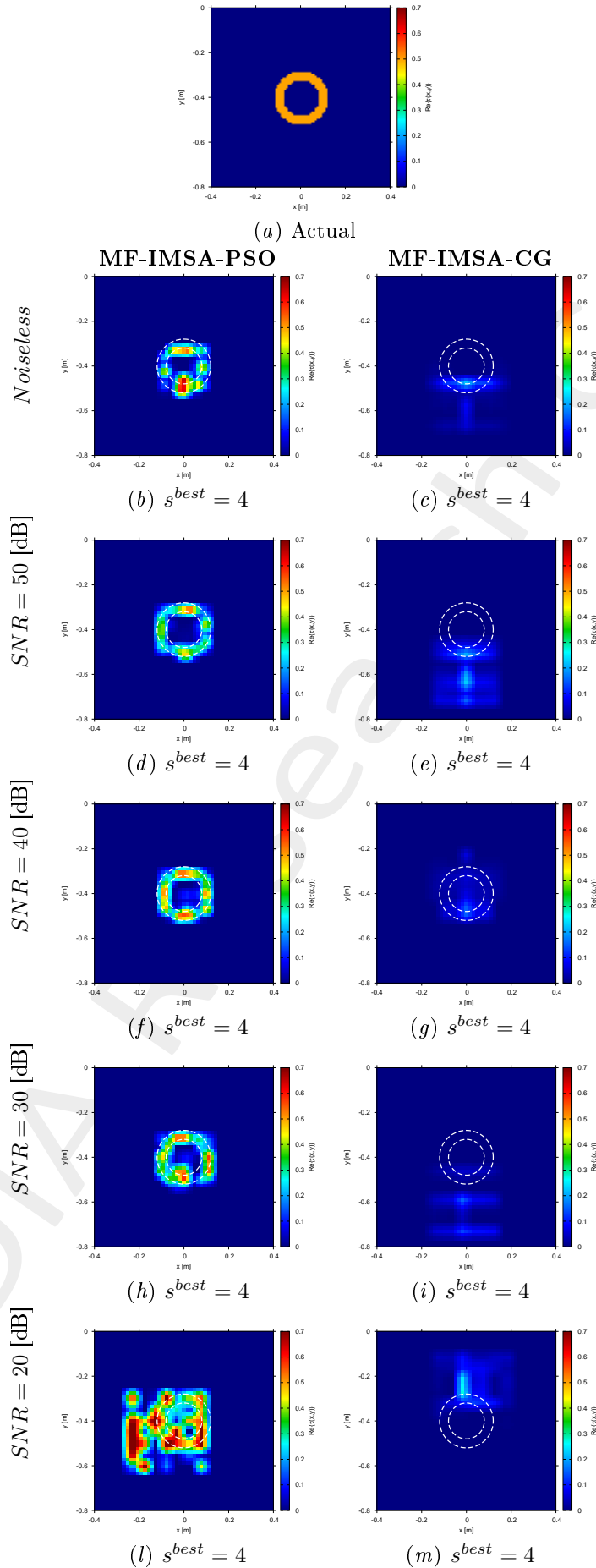
$(l)$ $s^{best} = 4$        $(m)$ $s^{best} = 4$

Figure 5: $MF - IMSA - PSO$ vs. $MF - IMSA - CG$: Retrieved dielectric profiles at the $IMSA$ convergence step ($s^{best}$).

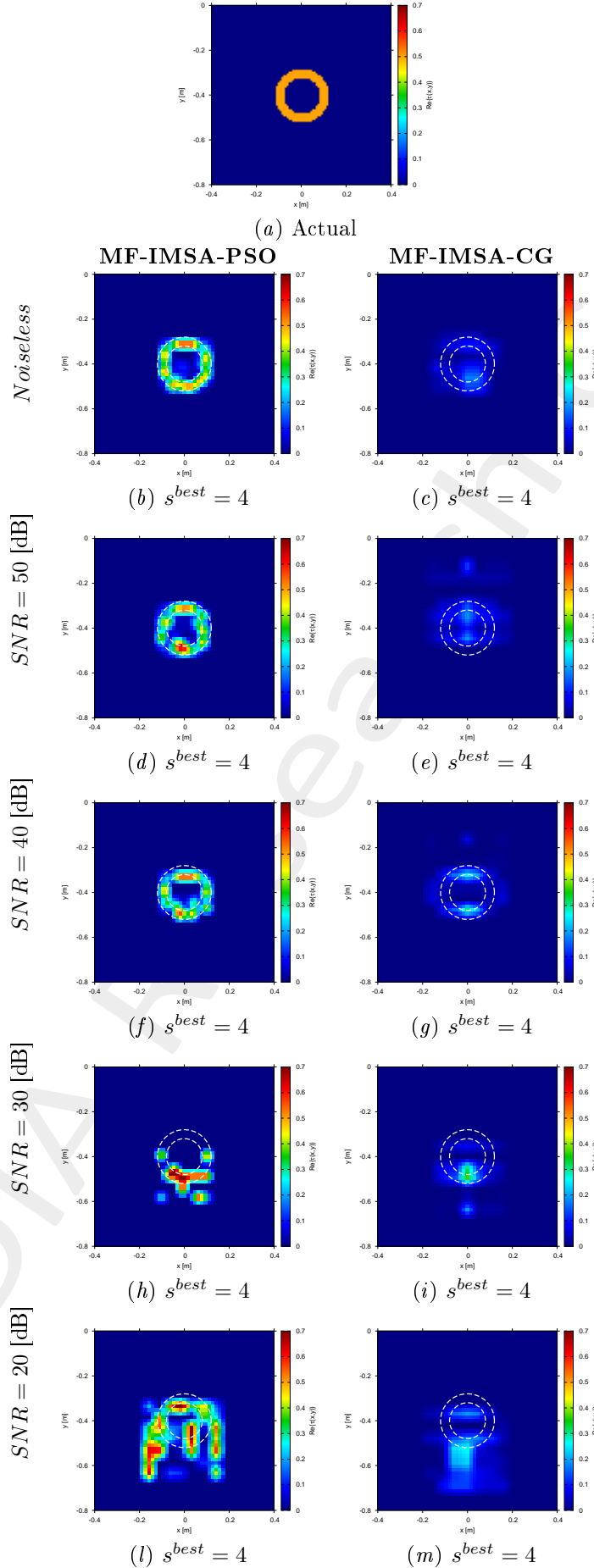## 2.1.4   $M = 36$ - $MF - IMSA - PSO$ vs. $MF - IMSA - CG$: **Final reconstructions**



(*a*) Actual

**MF-IMSA-PSO**          **MF-IMSA-CG**



(*b*) $s^{best} = 4$          (*c*) $s^{best} = 4$

(*d*) $s^{best} = 4$          (*e*) $s^{best} = 4$

(*f*) $s^{best} = 4$          (*g*) $s^{best} = 4$

(*h*) $s^{best} = 4$          (*i*) $s^{best} = 4$

(*l*) $s^{best} = 4$          (*m*) $s^{best} = 4$

Figure 6: $MF - IMSA - PSO$ vs. $MF - IMSA - CG$: Retrieved dielectric profiles at the $IMSA$ convergence step ($s^{best}$).

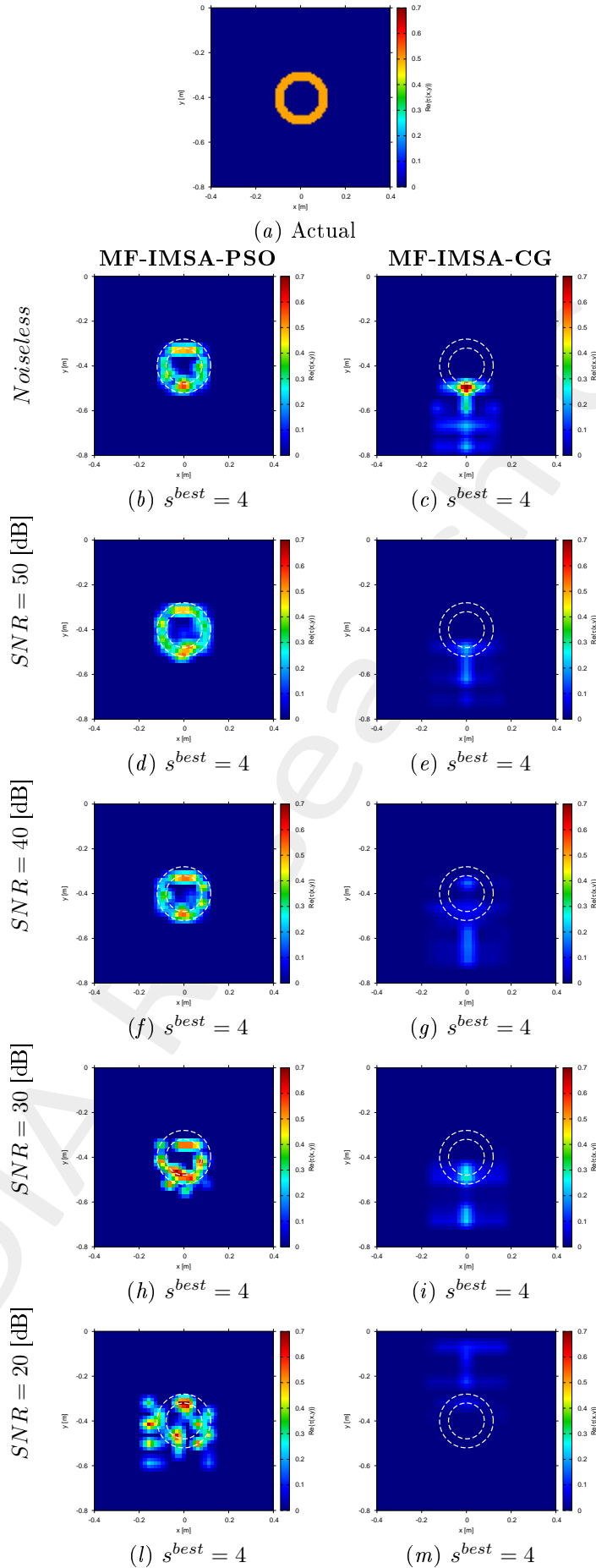**2.1.5** $M = 72$ - $MF - IMSA - PSO$ **vs.** $MF - IMSA - CG$**: Final reconstructions**



(*a*) Actual

**MF-IMSA-PSO**   **MF-IMSA-CG**



(*b*) $s^{best} = 4$   (*c*) $s^{best} = 4$

(*d*) $s^{best} = 4$   (*e*) $s^{best} = 4$

(*f*) $s^{best} = 4$   (*g*) $s^{best} = 4$

(*h*) $s^{best} = 4$   (*i*) $s^{best} = 4$

(*l*) $s^{best} = 4$   (*m*) $s^{best} = 4$

Figure 7: $MF - IMSA - PSO$ vs. $MF - IMSA - CG$: Retrieved dielectric profiles at the $IMSA$ convergence step ($s^{best}$).

11

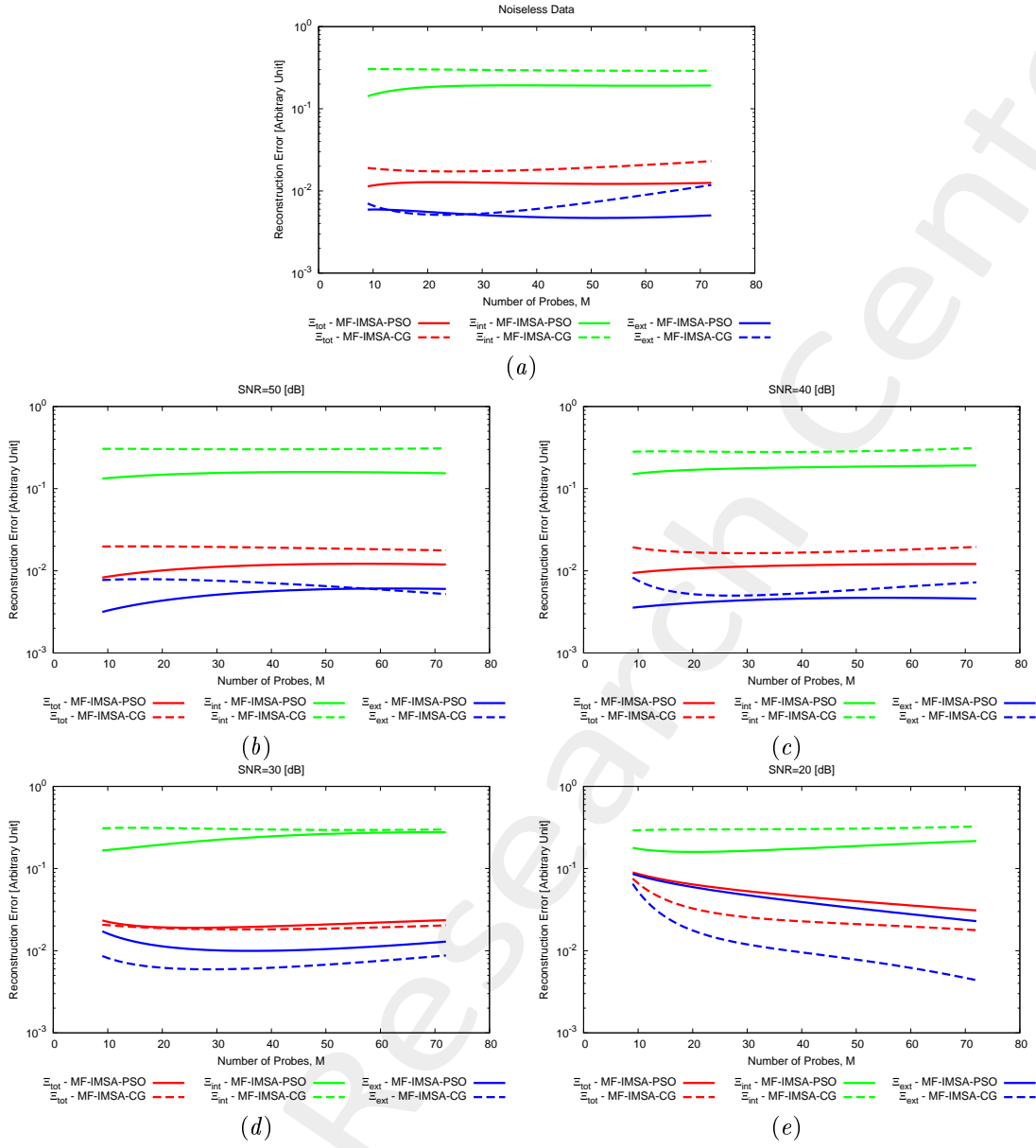### 2.1.6 $MF-IMSA-PSO$ vs. $MF-IMSA-CG$: Errors vs. $M$



Figure 8: $MF-IMSA-PSO$ vs. $MF-IMSA-CG$: Reconstruction errors vs. the number of measurement points ($M$).
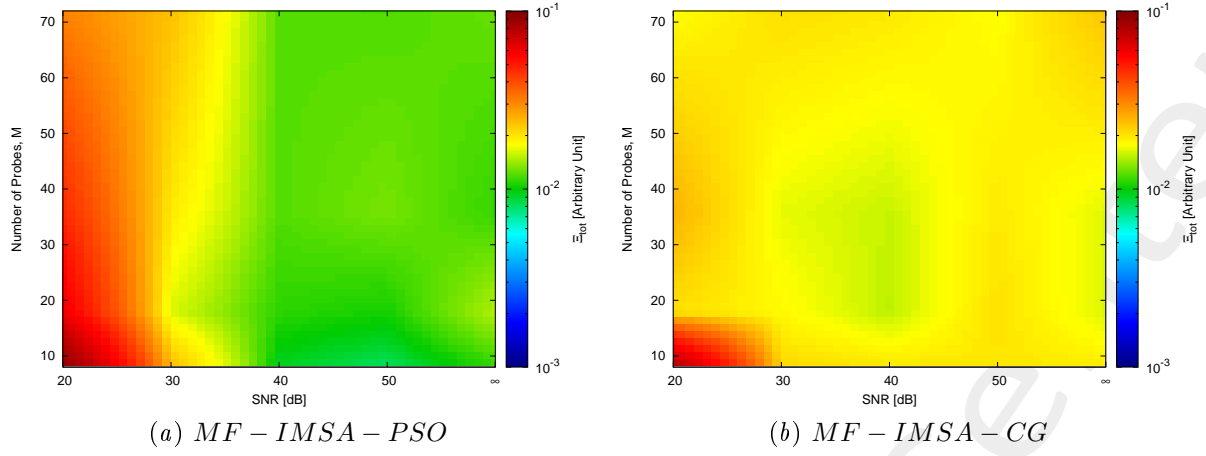
(a) $MF - IMSA - PSO$

(b) $MF - IMSA - CG$

Figure 9: $MF - IMSA - PSO$ vs. $MF - IMSA - CG$: Total reconstruction error vs. the number of measurement points ($M$) and vs. $SNR$.

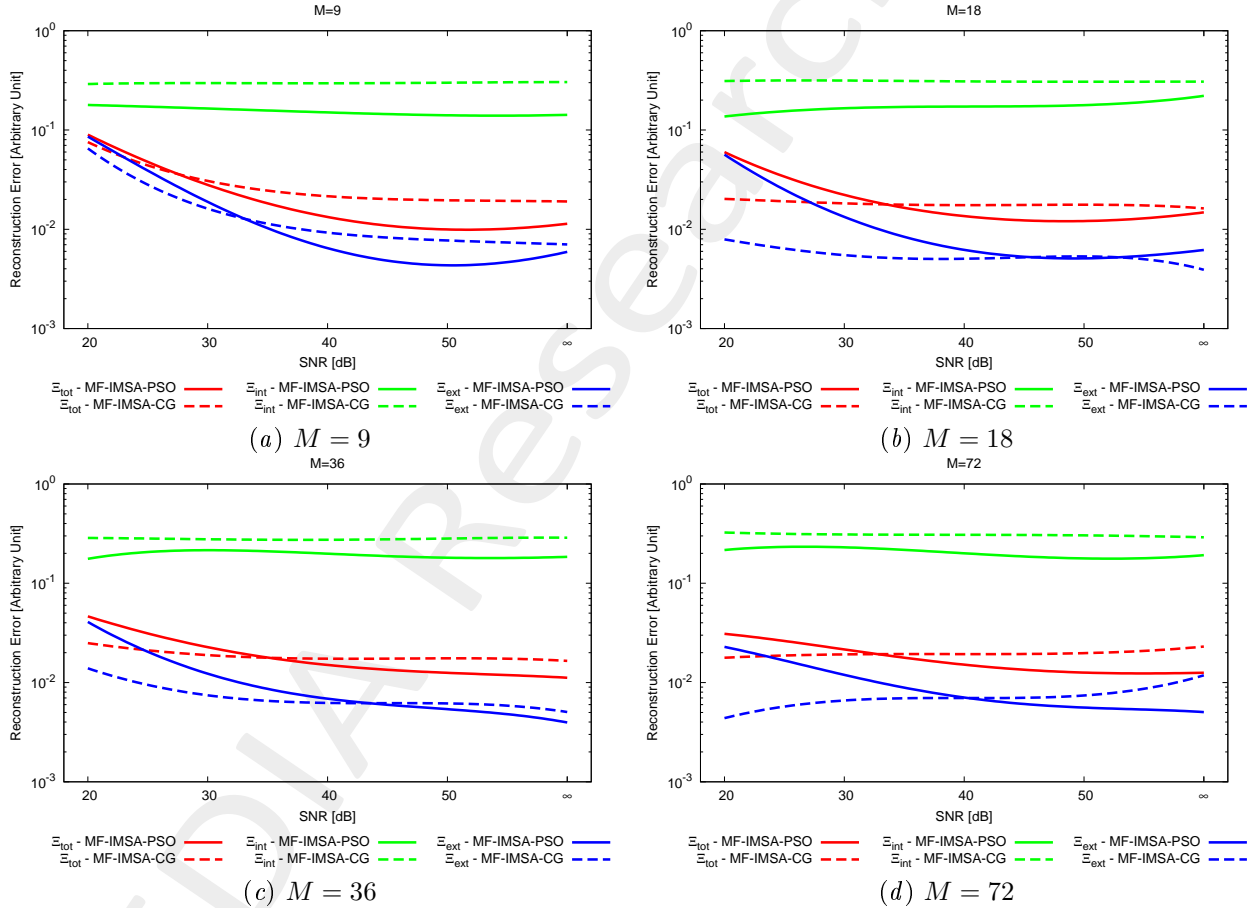### 2.1.7 $MF - IMSA - PSO$ vs. $MF - IMSA - CG$: Errors vs. $SNR$



(a) $M = 9$

(b) $M = 18$

(c) $M = 36$

(d) $M = 72$

Figure 10: $MF - IMSA - PSO$ vs. $MF - IMSA - CG$: Reconstruction errors vs. $SNR$.

13

# 3 Conclusions

The reported results in this document verify that

- The $MF - IMSA - PSO$ is able to provide accurate reconstructions even when considering a limited number of measurement points (e.g., when $M = 9$);

- Moreover, especially when noisy data has to be inverted, increasing the number of measurement points leads to a slight improvement of the reconstruction quality of the $MF - IMSA - PSO$;

- On average, significanlty better reconstructions are yieled by the proposed $MF - IMSA - PSO$ with respect to the $MF - IMSA - CG$. As a matter of fact, the improved performance of the $MF - IMSA - PSO$ is given by the exploitation of a stochastic global optimization algorithm, that allows a better exploration of the $MF$ cost function with respect to local search-based approaches.

# References

[1] P. Rocca, M. Benedetti, M. Donelli, D. Franceschini, and A. Massa, "Evolutionary optimization as applied to inverse problems," *Inverse Probl.*, vol. 25, pp. 1-41, Dec. 2009.

[2] P. Rocca, G. Oliveri, and A. Massa, "Differential Evolution as applied to electromagnetics," *IEEE Antennas Propag. Mag.*, vol. 53, no. 1, pp. 38-49, Feb. 2011.

[3] M. Salucci, G. Oliveri, and A. Massa, "GPR prospecting through an inverse scattering frequency-hopping multi-focusing approach," *IEEE Trans. Geosci. Remote Sens.*, vol. 53, no. 12, pp. 6573-6592, Dec. 2015.

[4] M. Salucci, L. Poli, and A. Massa, "Advanced multi-frequency GPR data processing for non-linear deterministic imaging," *Signal Processing - Special Issue on 'Advanced Ground-Penetrating Radar Signal-Processing Techniques,'* vol. 132, pp. 306-318, Mar. 2017.

[5] M. Salucci, L. Poli, N. Anselmi and A. Massa, "Multifrequency particle swarm optimization for enhanced multiresolution GPR microwave imaging," *IEEE Trans. Geosci. Remote Sens.*, vol. 55, no. 3, pp. 1305-1317, Mar. 2017.

[6] A. Massa, P. Rocca, and G. Oliveri, "Compressive sensing in electromagnetics - A review," *IEEE Antennas Propag. Mag.*, pp. 224-238, vol. 57, no. 1, Feb. 2015.

[7] A. Massa and F. Texeira, Guest-Editorial: Special Cluster on Compressive Sensing as Applied to Electromagnetics, *IEEE Antennas Wireless Propag. Lett.*, vol. 14, pp. 1022-1026, 2015.

[8] N. Anselmi, G. Oliveri, M. Salucci, and A. Massa, "Wavelet-based compressive imaging of sparse targets," *IEEE Trans. Antennas Propag.*, vol. 63, no. 11, pp. 4889-4900, Nov. 2015.

[9] G. Oliveri, N. Anselmi, and A. Massa, "Compressive sensing imaging of non-sparse 2D scatterers by a total-variation approach within the Born approximation," *IEEE Trans. Antennas Propag.*, vol. 62, no. 10, pp. 5157-5170, Oct. 2014.

[10] T. Moriyama, G. Oliveri, M. Salucci, and T. Takenaka, "A multi-scaling forward-backward time-stepping method for microwave imaging," *IEICE Electron. Expr.*, vol. 11, no. 16, pp. 1-12, Aug. 2014.

[11] T. Moriyama, M. Salucci, M. Tanaka, and T. Takenaka, "Image reconstruction from total electric field data with no information on the incident field," *J. Electromagnet. Wave.*, vol. 30, no. 9, pp. 1162-1170, 2016.

[12] F. Viani, L. Poli, G. Oliveri, F. Robol, and A. Massa, "Sparse scatterers imaging through approximated multi-task compressive sensing strategies," *Microw. Opt. Technol. Lett.*, vol. 55, no. 7, pp. 1553-1557, Jul. 2013.

[13] M. Salucci, N. Anselmi, G. Oliveri, P. Calmon, R. Miorelli, C. Reboud, and A. Massa, "Real-time NDT-NDE through an innovative adaptive partial least squares SVR inversion approach," *IEEE Trans. Geosci. Remote Sens.*, vol. 54, no. 11, pp. 6818-6832, Nov. 2016.

[14] L. Poli, G. Oliveri, and A. Massa, "Imaging sparse metallic cylinders through a local shape function bayesian compressing sensing approach," *J. Opt. Soc. Am. A*, vol. 30, no. 6, pp. 1261-1272, Jun. 2013.

[15] M. Donelli, D. Franceschini, P. Rocca, and A. Massa, "Three-dimensional microwave imaging problems solved through an efficient multiscaling particle swarm optimization," *IEEE Trans. Geosci. Remote Sensing*, vol. 47, no. 5, pp. 1467-1481, May 2009.